Enhanced magnetic properties of Mn-Ni codoped cobalt ferrite nanoparticles corroborated with microstructural analysis

S. Chakrabarty, M. Pal and A. Dutta*

S. Chakrabarty: Address: *Department of Physics, The University of Burdwan, Burdwan-713 104, India; email: sabyayan83@gmail.com* ; Ph. No.: 09477356295.

M. Pal: Address: *Sensor and Actuator Division, CSIR-Central Glass & Ceramics Research Institute, Kolkata-32, India;email:palm@cgcri.res.in; Ph. No.: 09433066938.*

Author for correspondence: A. Dutta*: Address: *Department of Physics, The University of Burdwan, Burdwan-713 104, India; email: adutta@phys.buruniv.ac.in;Ph.No.:09433116188*

Abstract:

Magnetic nanoparticles including ferrites are very potential candidatesfor its versatileapplication in the fields of engineering, bio medicine and electronics. Here we report the enhancement of magnetic properties of Mn-Ni co-doped cobalt ferrite nanoparticles which have been synthesized using coprecipitation technique. TEM study depicts the single phase nanocrystalline ferrite formation. Cation distribution between the tetrahedral and octahedral sites changes due to doping which is responsible for enhancement of magnetic properties. An exhaustive Rietveld analysis confirmed the rearrangement of the cations between the tetrahedral and octahedral sites. Also the results suggests strengthening of A–B and A–A interactions while weakening of B–B interaction for doped sample. "Law of Approach" technique is found to be usefuland utilized to extract the detailof magnetic parameters like anisotropy constant, anisotropy field, coercivity.

Keywords: Precipitation; Nanostructured materials; TEM; X-ray diffraction; Crystal structure and microstructure; Magnetic measurements.

1. Introduction:

In the field of ferromagnetic ceramic,particularly spinel ferrite nanparticles have been studied extensively due to their remarkable properties such as high saturation magnetization, large permeability at high frequency and remarkably high electrical resistivity [1-3]. Due to their low eddy current losses, there exist no other materials with such suitable properties for electronic applications in terms of power generation, conditioning, and conversion. Cobalt ferrite possesses excellent chemical stability, good mechanical hardness and a large positive first order crystalline anisotropy constant, making it a promising candidate for magneto optical recording media. In addition to precise control of the composition and structure of $CoFe_2O_4$, its practical application will require the capability to control particle size on the nanoscale [4-6]. Substitution of some other ions either in tetrahedral or octahedral sites in the

system can tailor the physical, chemical and magnetic properties. Cobalt ferrite (CFO) in bulk form normally exhibit inverse spinel structure with one half of Fe^{3+} ions in the A sites and the remaining half of Fe^{3+} ions along with Co^{2+} ions in the B sites having strong AB (Fe−Fe) superexchange (antiferromagnetic) interaction. For cobalt ferrite nanoparticles the cationic states and distribution may not be so simple as bulk one. Interestingly, Co^{3+} along withCo^{2+} and Fe^{2+}/Fe^{3+} can exist in both the A and B sites i.e. mostly mixed spinel state depending on the preparatory conditions [7]. Distribution of divalent and trivalent cations between the tetrahedral and octahedral sites in spinel ferrites can be expressed with formula $(A^{2+}_{\delta}\ B^{3+}_{1-\delta})_O[A^{2+}_{1-\delta}\ B^{3+}_{1+\delta}]_T O_4$, where δ is the degree of inversion. For normal ferrite δ is 1 whereas δ is 0 for inverse spinel structure. In a mixed spinel structure with δ between 1 and 0 both the tetrahedral and octahedral sublattice sites are occupied by divalent and trivalent ions.

Since the cation distribution among the lattice sites is strongly dependent on the materials preparation, it is very important to determine the cation site occupancies as well as the structural parameters in order to tailor the materials performance. In this work we report the effect of co-doping of Mn and Ni by 5 % each in place of Fe ions in cobalt ferrite nanoparticles and investigate the change in properties as well as established a probable correlation between magnetic properties and structural parameters.

2. Experimental:

2.1. Sample preparation:

The pure, Mn-Ni codoped cobalt ferrite nanoparticles were prepared by mixing reagent grade chemicals procured from MERCK. Proportionate amounts of ferric nitrate ($Fe(NO_3)_3$, $9H_2O$) , cobalt nitrate ($Co(NO_3)_2$, $6H_2O$) , manganese nitrate ($Mn(NO_3)_2$, xH_2O), nickel nitrate ($Ni(NO_3)_2$, $6H_2O$) and NaOH (98 %) were used as precursors. The nitrates were dissolved in de ionized water to get a solution. Nitrate solutions were mixed together

and stirred for one hour. NaOH solution was added for precipitation. Then the precipitate was washed several times with distilled water followed by acetone and dried at room temperature. Dried powders were annealed at 773K for 30 minutes to grow the nanoparticles. Pure cobalt ferrite sample and Mn-Ni co doped sample will be abbreviated hereafter as CFO and CFMNO respectively.

2.2. Sample characterization:

X-ray diffractograms of the samples were recorded by X Pert Pro X-ray diffractometer (PANLYTICAL, Almelo, The Netherlands) fitted with nickel filter using Cu K_α radiation (λ= 1.5414 Å) in 2θ range from 20^0 to 90^0. The Transmission electron microscopy (TEM) analyses for all the samples were carried out using a JEOL-200FX microscope operated at 200 KV. For TEM study the samples were ground in an agate mortar, dispersed in ethanol by sonication and were cast one drop on a carbon coated copper grid.Magnetic properties were measured at room temperature using a Lake Shore (Model 7410) vibrating sample magnetometer (VSM). The maximum field used was 1.5 Tesla.

2.3. XRD Rietveld refinements:

Detailed structural and microstructural characterization has been carried out using modified Rietveld method employing the software MAUD (2.33 version) [8]. The MAUD software can effectively characterize the material which contain anisotropy of size and strain which in turn causes the diffraction profiles to broaden. The effective crystallite size (d_c) and the root mean square microstrain($<\varepsilon^2>^{1/2}$) were evaluated using the Popa model [9]. The background is corrected using 5^{th} degree polynomial. The instrumental resolution parameters for peak asymmetry, instrumental broadening etc. were taken of the corundum standard powder. To generate the theoretical X-ray powder diffraction patterns the following phase of cobalt ferrite was considered:

$CoFe_2O_4$ (Cubic, space group: Fd-3m (227), a= 8.35 Å (C.O.D. ID 5910063) with Wyckoff positions for A site, B site and O^{2-} are 8*a*, 16*d* and 32*e* respectively.)

In order to provide figures of merit for the performance of the Rietveld method at the different refinement stages, indexes known as *R* factors are usually used. The criteria used to determine the quality of the fit indicates the evolution of the refinement and help to decide if the proposed model is adequate or not. However, just a single parameter is not enough to evaluate the refinement [10]. So it is important to have several indicators to perform each of the refinements. Different parameters appear in the literature to evaluate the quality of the fit [11]. As a convention, the parameters called weighted pattern (R_{wp}), goodness of fit (*GoF*) and expected factor (R_{exp}) are used. These parameters are defined as:

$$R_{wp}=\sqrt{\frac{\sum w_n(Y_{o,n}-Y_{c,n})^2}{\sum w_n(Y_{o,n}-Bkg_n)^2}} \quad (1)$$

$$G.O.F=\sqrt{\frac{\sum w_n(Y_{o,n}-Y_{c,n})^2}{N-P}} \quad (2)$$

$$R_{exp}=\frac{R_{wp}}{G.O.F} \quad (3)$$

where $Y_{o,n}$ and $Y_{c,n}$ are the observed and calculated data at point *n,* respectively*;* Bkg_n, is the background at data point *n;* *N*is the number of data points; *P*is the number of parameters and w_n the weighting factor given to data point *n*. In counting statistics, this last factor is given by $w_n=1/\sigma(Y_{o,n})^2$, where $\sigma(Y_{o,n})$ is the error in $Y_{o,n}$. Both R_{wp} and *GoF* are good global indicators of the refinement process, since the numerators of these factors contain the residual function which is being minimized. A rather good refinement is represented by low values of these parameters; conventionally, R_{wp} around 0.10 and *GoF*around 1 for XRD study [12].

3. Results and discussion:

3.1. TEM analysis:

Transmission electron microscopy (TEM) was utilized to get the morphology, microstructuralinformation and evaluate the average particle size of prepared samples. Fig. 1 (a) shows the typical TEM micrograph of pure CFO sample indicating well dispersed nanoparticles mostly of nearly spherical shape. Fig. 1 (b) shows the corresponding particle size distribution using log normal fitting following a standard procedure [13] indicating the sizes of the particles around 11 nm. Information about the crystalline phases of the material has been extracted from the selected area diffraction pattern (SAED) and HRTEM pictures. Rings made of discreet spots in SAED pattern (Fig. 1 (c)) indicates the highly crystalline nature of the material and shows good agreement with standard JCPDS data (card no # 221086). The distances between two adjacent planes estimated from HRTEM image (Fig. 1 (d)) corresponds to the (311) plane of CFO phase.

3.2. Proposition of cationic model and Rietveld refinements:

From the magnetic measurements we can see that the saturation magnetization is increased in case of the doped sample (Fig. 2).It is well known that the magnetic properties of spinel ferrites depend on the vector sum of the magnetic moments at tetrahedral (A) and octahedral [B] sites which are aligned in antiparallel fashion [14].The distribution of cations among the lattice sites is strongly dependent on the materials preparatory condition [15]. Therefore cation distribution model is a necessity to explain the changes in the magnetic as well as structural microstructural properties. It will be useful to use this model to start with Rieveld refinements to extract microstructural parameters for the present system. In our previous work we reported the enhancements in the magnetic properties of doped cobalt ferrite nanoparticles with the help of a cation distribution model. As the system is a similar one, we employed the same model to explain the modifications in the materials properties [16]. Different aspects like charge neutrality, total site occupancies and occupancy constraints

of each cation, difference of total magnetic moments for each siteetc. had to be considered to propose a particular model which will be appropriate for both the magnetic and XRD analysis. The proposed model for the present system is:

$$(Co^{2+}_{0.1+\delta}Fe^{3+}_{0.9-\delta})_T\,[Co^{3+}_{0.5}Co^{2+}_{0.4-\delta}Fe^{3+}_{0.6+\delta}Fe^{2+}_{0.4}X^{2+}_{0.1}]_O O_4^{2-}$$

Where X is the divalent states of Fe ions for pure cobalt ferrite and Mn^{2+} and Ni^{2+} ions by 5 % each for the doped sample and δ is the inversion factor. We have considered the trivalent state of Co ion in B site and had to therefore consider the divalent Fe state to maintain the natural balance: $Co^{3+} + Fe^{2+} \leftrightarrow Co^{2+} + Fe^{3+}$ [17]. Here only B site occupancies of Mn^{2+} and Ni^{2+} were observed, even allowing some tetrahedral preferences of some Mn^{2+} and Ni^{2+} ions, the system converged to zero for A site occupation for these ions. Calculated fraction of different ions between two different sites has been shown in Table 1. Calculated cation distribution from Rietveld analysis along with VSM analysis suggests that due to the addition of Mn^{2+} and Ni^{2+} ions in the B site, Co^{2+} ions migrate from B site to A site and hence Fe^{3+} ions from A site to B site in different amounts to account for the increment of saturation magnetization.

XRD pattern with Rietveld refinement of CFMNO sample is shown in Fig. 3. Rietveld refinement parameters along with crystallite sizes (D_{eff}) and TEM (D_{TEM}) analysis are enlisted in Table 2. We can see the crystallite sizes and particle sizes estimated from XRD analysis and TEM are in close correspondence. Table3 includes the cell parameter, cell volume, microstrain ($<\varepsilon^2>^{1/2}$). It was thought that cell parameter was increased due to substitution of Fe^{2+} ion in the B site having smaller ionic radius (0.75 Å) with larger (Mn^{2+}(0.81 Å) and Ni^{2+} (0.83 Å)) octahedral site. In addition, an increase in lattice strain is observed in the doped samples which also arise due to different ionic radii in the lattice sites. Theoretical X-Ray density (Table 3) calculated [18] using $d_X=8M/Na$shows a decrease as increase of lattice parameter with no significant change in the molecular weight (M) of the

samples because the atomic weights of Fe, Mn and Ni ions are very close to each other and the doping percentages are very small.

Different structural parameters like tetrahedral edge (E_{dt}), shared octahedral edge (E_{dso}) and unshared octahedral edge (E_{duo}), tetrahedral (r_A) and octahedral radii (r_B) have been calculated using eqns. 4 to 8 as follows:

$$E_{dt} = a\sqrt{2}\,(2u - \tfrac{1}{2}) \quad (4)$$

$$E_{dso} = a\sqrt{2}\,(1 - 2u) \quad (5)$$

$$E_{duo} = a\sqrt{(4u^2 - 3u + \tfrac{11}{16})} \quad (6)$$

$$r_A = a\sqrt{3}\,(u - \tfrac{1}{4}) - r\,(O^{2-}) \quad (7)$$

$$r_B = a\,(\tfrac{5}{8} - u) - r\,(O^{2-}) \quad (8)$$

where $r\,(O^{2-})$ is the radius of the oxygen ion (1.32Å) and u is the oxygen parameter and a is the lattice parameter. $a\sqrt{3}\,(u - \frac{1}{4})$ and $a\,(\frac{5}{8} - u)$ in eqns. (7) and (8) are the average tetrahedral and octahedral bond lengths. Calculated values of u, r_A,r_B, E_{dt} , E_{dso} , E_{duo} for different compositions are listed in Table 4.The values of metal-metal (M_e–M_e) and metal-oxygen (M_e–O) bond lengths were calculated using the following sets of equations:

Bond lengths:

M_e– M_e:

$$b = \frac{a\sqrt{2}}{4} \quad (9)$$

$$c = \frac{a\sqrt{11}}{8} \quad (10)$$

$$d = \frac{a\sqrt{3}}{4} \quad (11)$$

M_e– O:

$$p = a\sqrt{\frac{1}{16} - \frac{\delta}{2} + 3\delta^2} \quad (14)$$

$$q = a\sqrt{3}\,(\tfrac{1}{8} + \delta) \quad (15)$$

$$r = a\sqrt{3}\,(\tfrac{1}{4} + \delta) \quad (16)$$

$$e = \frac{3a\sqrt{3}}{8} \quad (12)$$

$$s = a\sqrt{\frac{3}{16} + \frac{\delta}{2} + 3\delta^2} \quad (17)$$

$$f = \frac{a\sqrt{6}}{4} \quad (13)$$

Also bond angles θ_1 to$\theta_5$can be calculated using simple trigonometric relations [16]. Here *b, c, d, e, f, p, q, r, s* are the parameters of ion pair distances associated with angles θ_1 toθ_5 in spinel ferrites which are pictorially depicted in Fig. 4 and δ is the deviation of the oxygen positional parameter from ideal positional parameter which is 0.375 for ideal spinel structures i.e. $\delta = u - u_{ideal} = u - 0.375$. Calculated composition wise results are shown in Table 5 (a) and Table 5 (b).Bond length is inversely proportional while bond angle is directly proportional to overall strength of magnetic interaction. It is clear from the Table 5 (b) that θ_1, θ_2 and θ_5 decrease while θ_3 and θ_4 increases with Mn and Ni doping. The increase in the angles suggest strengthening of A–B and A–A interactions while decrease in angle indicate weakening of B–B interaction [19]. This is attributed to the migration of cations due to the doping reflected in our calculated structure.

3.4.VSM analysis:

The M–H hysteresis measurements were carried out at room temperature for all the prepared samples and presented in Fig. 5. It was observed that saturation magnetization is increased from 40 emu/gm to 48 emu/gm in case of doped sample. This behavior is attributed to the migration of Co^{2+} ions from B site to A site and hence Fe^{3+} ions from A site to B site in calculated by our model and supported by Rietveld refinement. Detailed magnetic analysis was carried out using the Law of Approach (L.A.). Information about the cubic anisotropy constant, which describes the dependence of magnetization *M* on the applied magnetic field for$H>H_c$.The magnetization near the saturation magnetization near the saturation magnetization M_{SLA} can be written as

$$M = M_s\left[1 - \frac{8K_1^2}{105\,\mu_0^2 M_s^2 H^2}\right] + \kappa H \qquad (18)$$

where$M$ is the magnetization near the saturation magnetization, H is the applied magnetic field, M_S is the saturation magnetization, μ_0 is the permeability of the free space, K_1 is the cubic anisotropy constant and the term κH is known as the forced magnetization. The forced magnetization is caused by a linear increase in the spontaneous magnetization especially at high fields. The numerical coefficient *8/105* applies to cubic anisotropy of random polycrystalline samples. In general, the forced magnetization term was found to be necessary to fit the hysteresis curves at higher temperatures and higher fields, hence in the present case it has been neglected. Typical L.A. fitting of CFMNO sample is shown in Fig. 5 (inset).For a cubic crystal with easy direction along the [100] direction the anisotropy field H_k can be calculated using the formula:

$$H_k = \frac{2K_1}{\mu_0 M_s} \qquad (19)$$

It is observed that the anisotropy field increases for the doped samples, which leads to increase in coercivity could be due to the rearrangement of cations between the two lattice sites in case of doped samples.Calculated values of saturation magnetization from our proposed model (M_{smod}), observed value of it from VSM (M_{svsm}), coercive field (H_c), anisotropy constant (K_1), remanence magnetization (M_r) and anisotropy field (H_k) are summarized in Table 6.

4. Conclusions:

We have prepared single phase pure and Mn-Ni codoped cobalt ferrite nanoparticles by co-precipitation technique. TEM analyses were used to determine the particle size and crystalline nature of the prepared samples. Rietveld analysis were carried out by proposing a suitable cation distribution model and structural microstructural parameters were determined

which suggests the migration of Co^{2+} ions from B site to A site and hence Fe^{3+} ions from A site to B site. Strengthening of A–B and A–A interactions while weakening of B–B interaction for doped sample were reflected in bond length and bond angle studies. The observed enhancement of magnetic properties for the doped sample can be explained in the light of cation distribution model proposed for the present system.

Acknowledgements:

S. Chakrabarty thanks The University of Burdwan for the infrastructural support. A. Dutta thankfully acknowledges the financial support of Department of Science and Technology (DST), Govt. of India (Grant no. SR/FTP/PS-141/2010) for carrying out this work.

References:

1. Q. Song and Z. J. Zhang, J. Phys. Chem. B 110, 11205**(2006)**.
2. M Pal, D Das, SN Chintalapudi,and D Chakravorty, J. Mater.Res. 15, 683 **(2000).**
3. S Dutta, SK Manik, M Pal, SK Pradhan, P Brahma and D Chakravorty, J. magn.magn.mater. 288, 301 **(2005).**
4. S. Chikazumi, Physics of Ferromagnetism, Oxford University Press, New York **(1997).**
5. J. Smith and H. P. J. Wijn, Ferrites, Philips Technical Library, Eindhoven, The Netherlands **(1965).**
6. Z. H. Zhou, J. Wang, J. M. Xue and H. S. O. Chan, J. Mater. Chem. 11, 3110 **(2001).**
7. M Veverka, Z Jirák, O Kaman, K Knížek, M Maryško,EPollert, K Závěta, ALančok, M Dlouhá and S Vratislav, Nanotech. 22,345701 **(2011).**
8. L. Lutterotti, MAUDWEB, Version 2.33, http://www.ing.unitn.it/~maud/news.html.
9. N.C. Popa, J. Appl. Crystallogr. 31, 176 **(1998).**

10. D. Balzar, in International Union of Crystallography Monographs on Crystallography, Edited R.L. Snyder, H.J. Bunge and J. Fiala, Oxford University Press, New York, **(1999)**, pp. 94-126.
11. R. Young, in The Rietveld Method, Edited R. Young, Oxford University Press, Oxford, **(1993)**, pp.1–38.
12. L. B. McCusker, R. B. Von Dreele, D. E. Cox, D. Louër and P. Scardi, J. Appl. Cryst. 32,36 **(1999).**
13. B. Roy, O. Mondal, D. Sen, J. Bahadur, S. Mazumder and M. Pal , J. Appl. Crystallogr.44, 991 **(2011).**
14. M. Arana, V. Galván, S. E. Jacobo and P. G. Bercoff, J. Alloys Compd. 568, 5 **(2013).**
15. L. Kumar and M. Kar, J. Exp. Nanosci. 9, 362 **(2014).**
16. S. Chakrabarty, A. Dutta and M. Pal, J. Alloys Compd. 625, 216 **(2015).**
17. Q. Wei, B.W. Robertson, J. Solid.State Chem. 176, 279 **(2003).**
18. R. Sharma and S. Singhal, Physica. B 414, 83 **(2013).**
19. R. C. Kambale, K. M. Song, Y. S. Koo and N. Hur, J. Appl. Phys. 110, 053910 **(2011).**

Table 1:Calculated cation distribution

Sample		A site		B site				
	δ							
ions		Co^{2+}	Fe^{3+}	Co^{3+}	Co^{2+}	Fe^{3+}	Fe^{2+}	$X^{2+}_{0.1}$
CFO	0.07	0.17	0.83	0.50	0.33	0.67	0.40	$Fe^{2+}_{0.1}$
CFMNO	0.15	.25	0.75	0.50	0.25	0.75	0.40	$Mn^{2+}_{0.05}Ni^{2+}_{0.05}$

Table2: Rietveld refinement parameters, crystallite sizes from Reitveld analysis (D_{eff}) and TEM (D_{TEM})

Composition	R_{exp}(%)	R_{wp}(%)	*G.O.F.*	D_{eff} (nm)	D_{TEM} (nm)	Avg*D* (nm)
CFO	3.38	3.93	1.16	11.50	10.62	11.06
CFMNO	3.26	3.66	1.12	11.12	11.23	11.18

Table 3: Composition wise values of cell parameter (*a*), Cell Volume (*V*), r.m.s. microstrain$<\varepsilon^2>^{1/2}$and X-ray density (d_X)

Composition	Cell parameter*a* (Å)	Cell Volume(*V*) ($Å^3$)	$<\varepsilon^2>^{1/2}(\times 10^{-3})$	d_X (gm/cc)
CFO	8.44	601.2	1.62	5.19
CFMNO	8.46	605.4	2.13	5.11

Table 4: Calculated values of u, r_A,r_B, E_{dt} , E_{dso} , E_{duo} for different compositions

Composition	u (Å)	r_A (Å)	r_B (Å)	E_{dt} (Å)	E_{dso} (Å)	E_{duo}(Å)
CFO	0.3754	0.5109	0.7866	3.048	3.028	2.983
CFMNO	0.3760	0.5262	0.7865	3.014	2.967	2.991

Table 5 (a:) Calculated values of parameters of ion pair distances.

Composition	p(Å)	q(Å)	r(Å)	s(Å)	b(Å)	c(Å)	d(Å)	e(Å)	f(Å)
CFO	2.105	1.833	3.660	3.656	2.983	3.502	3.654	5.481	5.169
CFMNO	2.106	1.846	3.677	3.668	2.991	3.507	3.663	5.494	5.180

Table 5 (b): Calculated values of bond angles θ_1, θ_2, θ_3, θ_4, θ_5

Composition	θ_1(deg)	θ_2(deg)	θ_3(deg)	θ_4(deg)	θ_5(deg)
CFO	125.38	142.37	90.22	125.38	75.34
CFMNO	124.96	142.14	90.48	125.46	75.01

Table 7 Calculated values of saturation magnetization from our proposed model (M_{smod}), observed value of it from VSM (M_{svsm}), coercive field (H_c), anisotropy constant (K_1), remanence magnetization (M_r) and anisotropy field (H_k).

Composition	M_{smod} (in μ_B)	M_{svsm} (emu/g)	M_{svsm} (in μ_B)	H_c(Oe)	K_1 (mJ/cc)	M_r (emu/g)	H_k(KOe)
CFO	1.68	39.7	1.67	420	0.4102	5.43	20.665
CFMNO	1.95	46.7	1.96	970	0.5163	14.72	21.618

Figure captions:

Fig. 1 (a).TEM micrograph of CFMNO sample.

Fig. 1 (b). Particle size distribution with log-normal fitting of the micrograph of fig 1 (a).

Fig. 1 (c). Selected area diffraction (SAD) pattern of CFMNO sample.

Fig. 1 (d). Lattice fringes of CFMNO sample obtained by HRTEM.

Fig. 2. First quadrant of hysteresis loop of prepared samples.

Fig. 3.XRD patterns of CFMNO sample with Reitveld fitting.

Fig. 4. Interionic distances in the spinel structure for the different types of lattice site interactions.

Fig. 5.M–H hysteresis loops of different samples at room temperature.

L.A. fit for CFMNO sampleis shown in inset.

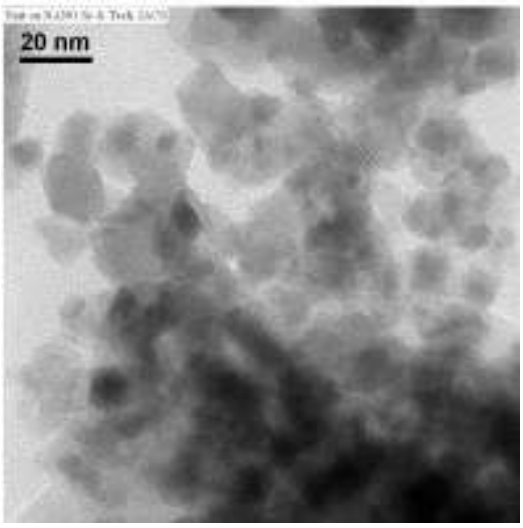

Fig. 1 (a)

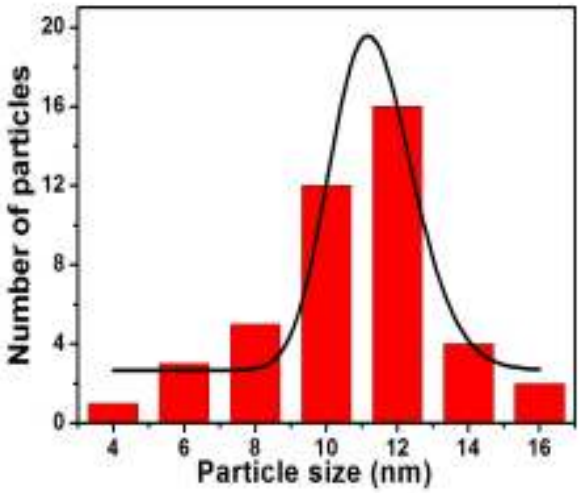
Number of particles
Particle size (nm)
0
4
8
12
16
20
4
6
8
10
12
14
16

Fig. 1 (b)

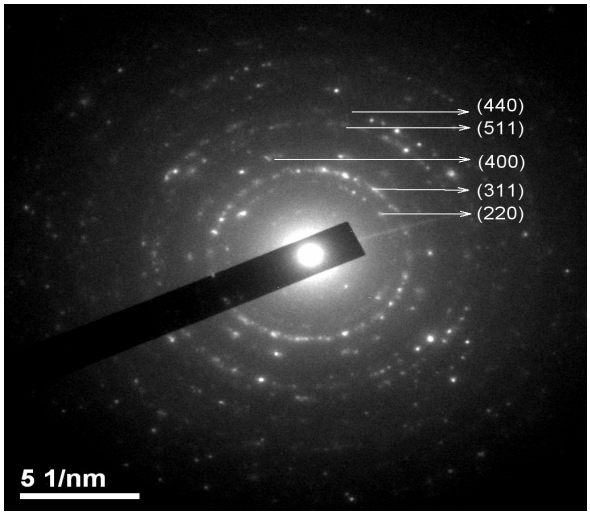

Fig. 1 (c)

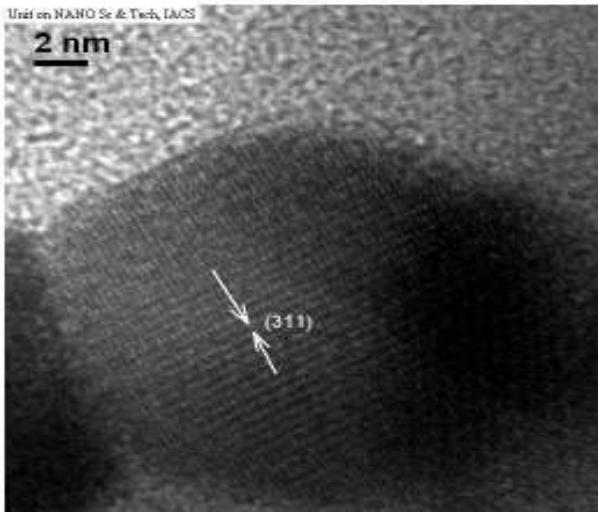

Fig. 1 (d)

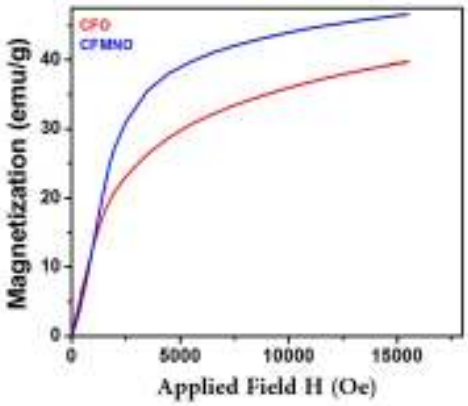
CFO
CFMNO
Magnetization (emu/g)
0
10
20
30
40
0
5000
10000
15000
Applied Field H (Oe)

Fig. 2

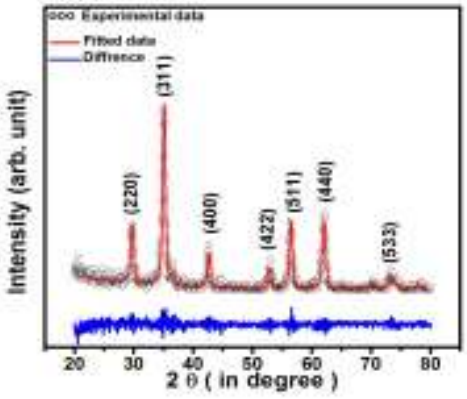
Experimental data
Fitted data
Difference
(220)
(311)
(400)
(422)
(511)
(440)
(533)
Intensity (arb. unit)
20
30
40
50
60
70
80
2 θ (in degree)

Fig. 3

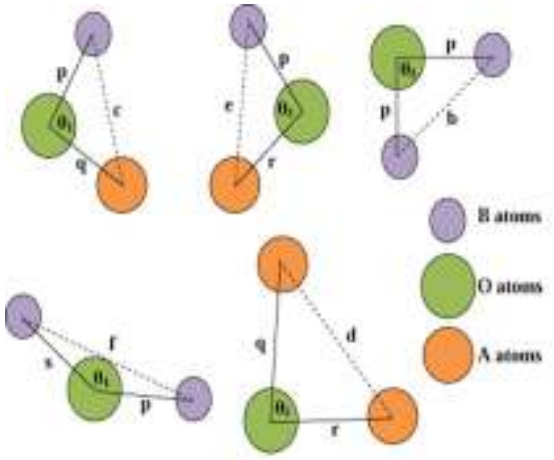

Fig. 4

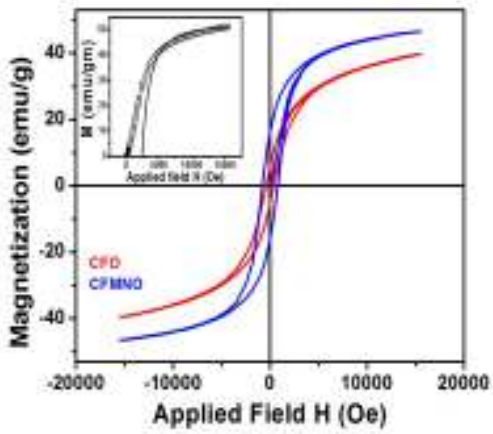
Magnetization (emu/g)
Applied Field H (Oe)
CFO
CFMNO
40
20
0
-20
-40
-20000
-10000
0
10000
20000

Fig. 5